Demonstration of high-repetition-rate tabletop soft-x-ray lasers with saturated output at wavelengths down to 13.9 nm and gain down to 10.9 nm

Y. Wang,[1] M. A. Larotonda,[1] B. M. Luther,[1] D. Alessi,[1] M. Berrill,[1] V. N. Shlyaptsev,[2] and J. J. Rocca[1]
[1]*NSF ERC for Extreme Ultraviolet Science and Technology, and Electrical and Computer Engineering Department, Colorado State University, Fort Collins, Colorado 80523, USA*
[2]*Department of Applied Science, University of California Davis—Livermore, Livermore, California 94551, USA*
(Received 6 October 2004; published 8 November 2005)

Saturated tabletop lasers operating at 5 Hz repetition rate with average powers >1 μW were demonstrated at wavelengths between 16.5 and 13.9 nm in the $4d\ ^1S_0-4p\ ^1P_1$ transitions of Ni-like ions. The results were obtained using picosecond laser heating pulses with an energy of only 1 J by optimizing the angle of incidence for maximum energy deposition. Lasing was also observed for shorter wavelength transitions of the same isoelectronic sequence, with amplification in the 11.9 nm line of Ni-like Sn approaching gain saturation, and progressively reduced gain for wavelengths as low as 10.9 nm for Ni-like Te. These high repetition rate soft x-ray lasers will enable new applications in science and the development of unique metrology and processing tools for industry.

DOI: 10.1103/PhysRevA.72.053807 PACS number(s): 42.55.Vc, 52.38.Ph

I. INTRODUCTION

Recognition of the unique properties of coherent soft x-ray radiation has motivated the construction of numerous multi-user synchrotron radiation facilities worldwide [1]. However, the widespread use of coherent soft x-ray light in numerous areas of science and technology remains relatively unexploited and requires the development of small-scale sources. Compact short wavelength sources can potentially make possible a variety of new studies of surfaces and materials, and enable the development of unique metrology and processing tools for industry. Significant progress towards the development of small-scale coherent soft x-ray sources has been made using two complementary schemes: soft x-ray lasers [2] and high harmonics [3]. Lasing in the gain saturation regime, necessary for efficient energy extraction, has been demonstrated for wavelengths as short as 5.9 nm in Ni-like dysprosium [4], but only at the very low repetition rate of a few shots per hour.

Significant effort has been placed in the development of high repetition rate soft x-ray lasers for applications [5–8]. Fast discharge excitation of capillary plasmas has produced extremely compact saturated lasers emitting at 46.9 nm in Ne-like Ar at repetition rates up to 10 Hz [5]. More recently, laser-driven optical field ionization lasers have produced saturated operation at 41.8 and 32.8 nm in Pd-like Xe and in Ni-like Kr, respectively [6]. A remaining challenge is the demonstration of saturated high repetition rate table-top lasers at shorter wavelengths. Saturated operation at a repetition rate of one shot every several minutes has been obtained at several wavelengths as low as 13.9 nm by transient collisional electron excitation of targets at normal incidence with 3–10 J of short pulse pump energy [9,10]. Different pumping configurations have been investigated to reduce the necessary pumping energy and enable operation at higher repetition rate. Transverse excitation of a Mo target with 150 fs, 300 mJ pulses impinging at 60° from normal incidence resulted in the appearance of the 18.9 and 22.6 nm laser lines of Ni-like Mo [11]. Longitudinal pumping at 10 Hz produced nonsaturated amplification at 18.9 nm in Ni-like Mo [12]. Recently, it has been demonstrated that in transverse excitation experiments the energy deposition efficiency of the short pulse can be significantly increased by directing it at grazing incidence [13–16]. This geometry, which inherently provides traveling wave pumping, increases the path length of the rays in the gain region of the plasma, thereby increasing the fraction of the pump energy absorbed in that region. Pumping of the 18.9 nm line of Ni-like Mo with 150 mJ of total pumping energy from a 10 Hz laser was reported to generate a gain-length product of ~ 14 [14], and the use of 1 J heating pulses resulted in operation in the gain-saturated regime and in the generation of 150 nJ soft x-ray laser pulses [15]. Several important applications, including the metrology necessary for extreme ultraviolet lithography at 13.5 nm [1], motivate the development of high average flux soft x-ray lasers at shorter wavelengths.

In this paper we report 5 Hz repetition rate operation of saturated table-top lasers in Ni-like Ru, Pd, and Ag ions at wavelengths of 16.5, 14.7, and 13.9 nm, respectively. Amplification was also observed for shorter wavelength transitions of the same isoelectronic sequence, with amplification in the 11.9 nm line of Ni-like Sn approaching gain saturation, and progressively reduced gain for wavelengths as low as 10.9 nm for Ni-like Te. The results were obtained by efficiently heating a precreated plasma with picosecond heating pulses of ~ 1 J energy directed at grazing incidence to optimize the energy deposition. The grazing incidence configuration takes advantage of the refraction of the pump beam in the plasma to efficiently deposit a large fraction of its energy into a preselected region of the plasma with optimum electron density for amplification. A remarkable property of refraction is that it allows us to precisely define this electron density based on only two parameters, the grazing incidence angle θ and the laser pump wavelength: $\theta=(n_e/n_{cp})^{1/2}$ [17], where n_e is the maximum electron density within the amplification region and n_{cp} is the critical density at the wave-

length of the pump. Hence when the grazing angle is changed, different parts of the density profile formed by the prepulse are preferentially heated. At a given incidence angle the pump beam is reflected at the point where it encounters the corresponding selected density n_e, significantly increasing the path length of the pump beam and therefore allowing for a large fraction of the pump energy (typically 20% to 50%) to be absorbed into the gain region. In addition, the fact that the grazing incidence pumping is intrinsically the traveling wave for the range of incidence angles of interest simplifies the experimental setup.

The next section describes the experimental setup. Section III presents the experimental results and compares the laser output behavior to model simulations, which in turn are used to predict the pump energy necessary for lasing at shorter wavelengths.

II. EXPERIMENTAL SETUP

The experiments were conducted using an 800 nm Ti:sapphire pump laser system consisting of a mode-locked oscillator and three stages of chirped-pulse amplification. A Kerr mode-locked Ti:sapphire laser oscillator produces nanojoule pulses of about 50 fs duration that are stretched to about 180 ps by a grating expansor. The stretched pulses are subsequently amplified in a chain of three Ti:sapphire amplifiers. Eight passes through the first stage amplifier increase the pulse energy to about 2 mJ, while the pulse width narrows to about 120 ps. Further amplification to 2 J takes place in a five-pass second stage bow-tie amplifier and a final three-pass amplifier that is pumped by a 5 J frequency doubled Nd:YAG laser. A beam-splitter placed at the output of the third amplifier stage directs 20% of the laser energy to the prepulse arm (120 ps pulses), while the rest was compressed to ~8 ps in a vacuum grating compressor. Amplification of spurious light from the first stage amplifier produced an additional prepulse with an energy corresponding to a few percent of the total pump energy that preceded the main pulse by 6.7 ns. While this pump laser can operate at a repetition rate of 10 Hz in the present experiments the third stage amplifier was operated at 5 Hz to improve the pump beam mode quality.

The target irradiation configuration is shown in Fig. 1(a). The prepulse arm was focused onto the target surface using the combination of an $f=67.5$ cm focal length spherical lens and an $f=200$ cm focal length cylindrical lens to generate a 30 μm $\times$ 4.1 mm FWHM line focus. The short pulse was focused into a line of similar dimensions. For this purpose the short pulse was sent from the vacuum compressor to a multilayer-coated $f=76.2$ cm parabolic mirror placed at 7° from normal incidence. This allows the short pulse to impinge onto the target at 14° grazing incidence when the target is placed at normal incidence with respect to the prepulse arm. To obtain grazing-incidence angles greater than 14° the target was rotated about its center while maintaining the same prepulse and short pulse beam paths [Fig. 1(b)]. For example, to set a grazing-incidence pumping angle of 23°, the target was tilted by 9°. The overlap of the two line foci on target was monitored imaging the target onto a CCD. For

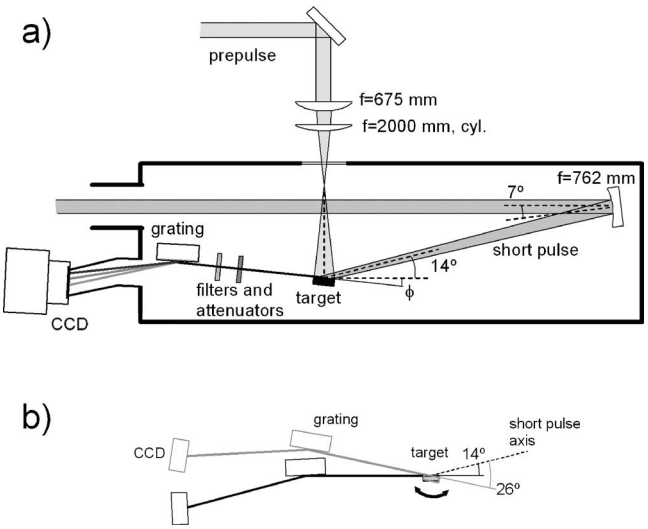

FIG. 1. (a) Schematic illustration of the pumping configuration and detection system. (b) Close-up of target and detection system rotation used to access different grazing incidence angles.

each grazing-incidence angle the astigmatism of the short pulse beam was adjusted such that the FWHM length of the line focus on the target would always equal 4.1 mm. For instance at 14° grazing incidence an astigmatic beam with a 1 mm FWHM major axis is required in order to form a 4.1 mm FWHM long line focus upon its intersection with the target plane. To maintain the same line focus length for operation at 26° the FWHM of the major axis of the astigmatic beam must be increased to 1.75 mm. This was accomplished by adjusting the distance between a pair of $f=+2$ m and $f=-2$ m cylindrical lenses placed immediately before the compressor. This pair creates a variable cylindrical lens with a focal length range from 20 to 100 m.

The grazing-incidence nature of the experiment results in a line focus that changes in width as a function of target length. In general the change in the line focus width along the target depends on the distance the beam propagates from the time it hits one edge of the target until it hits the other edge, L (given by the cosine of the grazing-incidence angle multiplied by the target length). In the limit case of normal incidence pumping the beam width is the same over the entire target while in the case of zero degree grazing incidence (longitudinal pumping) the change in the beam width is determined by the Rayleigh length of the beam and the length of the target. To characterize the line focus on the target surface we measured the change in the beam width as a function of the distance from the waist. The waist was measured to have a FWHM of 31 μm which increases to a FWHM of 41 μm at the edge of the target, 2 mm away from the waist. Therefore this effect causes an increase of ~30% in the focal width at the edge of the target with respect to the center for all angles used. Model simulations indicate the corresponding variation of pump intensity results in associated gain coefficient reduction of less than 10%. The effect on the laser output intensity is even smaller due to gain saturation. It should be noticed that line focus width also changes as the target is rotated to access different grazing incidence angles. However, since in our case the propagation distance

only changes from $L=3.88$ mm to $L=3.60$ mm as the angle is increased from 14° and 26°, the line focus width changes only by ~3% as the target is rotated.

The spectrally resolved on-axis plasma emission was recorded using a spectrograph composed of a 1200 lines/mm gold-coated variably spaced spherical grating placed at 24.7 cm from the end of the target and a back-illuminated 1 in.^{2} CCD detector positioned at 48 cm from the target. For each grazing-incidence angle used the grating was placed in the corresponding target plane at 3° grazing incidence. The dispersion direction was contained in a plane normal to the target surface. Measurements were conducted to evaluate the change of the grating collection efficiency caused by the increase in plasma refraction associated with the variation in grazing-incidence angle. For this purpose the variation of the collected soft x-ray laser intensity as a function of grating position was measured displacing the grating in the direction normal to the target plane. For the case of 26° grazing-incidence angle corresponding to maximum refraction, the maximum laser output signal was obtained displacing the grating by 1 mm from its original location in the plane of the target. For this displacement, which corresponds to a change in grating-incidence angle on the grating of 0.23°, the laser signal strength increased by 7%. The change in grating-diffraction efficiency associated with such small angle variations can be neglected. Therefore we can expect errors in soft x-ray laser intensity measurements associated with the variation of the collection efficiency to be less than 10 percent. Combinations of Zr filters and meshes of measured transmissivity positioned to avoid Moire patterns were used to reach attenuation factors up to 1500. To increase the accuracy of the determination of the soft x-ray laser output energy the trasmissivity of the filters used was measured using synchrotron radiation [18].

III. SOFT X-RAY LASER RESULTS AND DISCUSSION

Figure 2 shows on-axis spectra corresponding to 4 mm long targets of Ru ($Z=44$), Pd ($Z=46$), Ag ($Z=47$), Cd ($Z=48$), and Sn ($Z=50$) irradiated at a grazing-incidence angle of 20°, and Sb ($Z=51$) and Te ($Z=52$) targets irradiated at an increased grazing-incidence angle of 23°. The time delay between the two pulses was 500 ps for Ru, Pd, Ag, and Cd, and 150 ps for Sn, 100 ps for Sb, and 75 ps for Te. The targets were polished slabs with thickness of 1 mm for Ru and Pd, and 2 mm for Ag, Cd, and Sn. The Sb and Te targets consisted of a 1 μm thick film of these materials deposited on a polished Cu slab target using an intermediate Ti adhesion layer. Strong lasing was obtained in the $4d-4p$ lines of the Ni-like ions at 16.5, 14.7, 13.9, 13.2, and 11.9 nm, while significantly weaker laser output was observed for the 11.4 and 10.9 nm lines of Ni-like Sb and Te, respectively. The divergences in the direction perpendicular to the target were observed to range from 7–10 mrad. Figure 3 shows these results are in good agreement with the computed Z scaling of the main prepulse and short-pulse pump energies necessary for strong lasing with 20° grazing-incidence pumping. The computations were done using the code RADEX [19]. The model includes 1D expansion of laser-produced plasma under transverse prepulse and grazing-incidence main pulse, atomic kinetics, the refraction of the main pump pulse, and refraction of x-ray radiation pulse and its amplification computed taking into account the saturation of ASE signal. The computations predict that with the pump energies used in the experiment strong lasing should be obtained in all the ele-

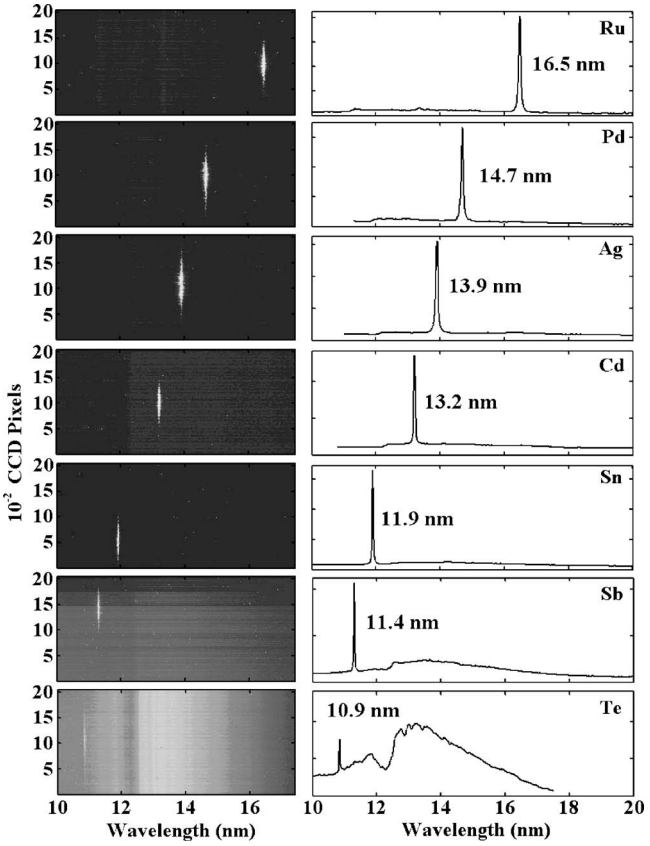

FIG. 2. Single shot on-axis spectra of 4 mm line focus plasmas showing lasing in the $4d\ ^1S_0-4p\ ^1P_1$ transition of the Ni-like ions at wavelengths ranging from 16.5 to 10.9 nm. The laser lines completely dominate the spectrum except in the case of Ni-like Te.

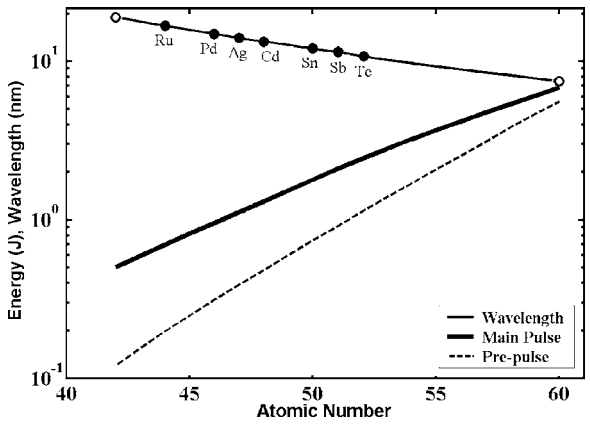

FIG. 3. Computed main pulse and prepulse pump energies necessary to pump the $4d\ ^1S_0-4p\ ^1P_1$ laser transition of Ni-like ions as a function of atomic number Z. The calculations are for a main pulse grazing incidence angle of 20° and 30 μm line focus width. The pump pulse durations are those used in the experiment.

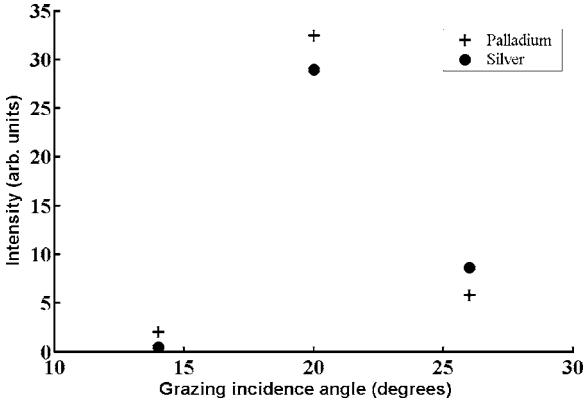

FIG. 4. Intensity as a function of pump pulse grazing incidence angle for the 14.7 nm line of Ni-like Pd and the 13.9 nm line of Ni-like Ag.

ments investigated up to Sn, for which the available pump energy starts to fall short of the predicted required amount. Extension of the results to $\lambda = 7.97$ nm in Ni-like Nd ($Z = 60$) is estimated to require ~ 7 J of short pulse pump energy.

To maximize the pump energy deposition in the gain region the angle of incidence θ, defined between the short pulse beam axis and the target surface, was varied between 14° and 26° (corresponding to an angle of 76° to 64° from the surface normal). Our model calculations show that as θ increases the electron temperature in the gain region remains practically constant, while, as expected, the electron density increases approximately as estimated from simple pump beam refraction considerations: $n_e = \theta^2 n_{cp}$ [17]. This shift of the amplification to a region of higher density results in an increased gain coefficient. The angle for maximum x-ray laser output energy is determined by the counterbalance between the increased gain coefficient, on one side, and the increased refraction, increased mismatch of the traveling wave pump velocity, and decreased gain duration, on the other. Results of the measured angular variation of the intensity of the 13.9 nm line of Ni-like Ag and the 14.7 nm line of Ni-like Pd are shown in Fig. 4. The data were obtained using ~ 0.35 J of main prepulse energy (2.4×10^{12} W/cm^2) and about 1 J (1×10^{14} W/cm^2) of short pulse energy impinging onto 4 mm long targets. At an angle of 14°, for which the pump energy is deposited in a region where the electron density is $\sim 1 \times 10^{20}$ cm^{-3}, stable lasing was observed in Ru and Pd. Lasing was also obtained in Ag, but the output was weaker and more erratic. The output intensity of all these laser lines was observed to increase significantly for an angle of 20°, for which refraction helps to better couple the pump beam into the region where the electron density is 2×10^{20} cm^{-3}. The optimum pumping angle for Ag was found to be 23°. A further increase of the angle to 26° caused a decrease of the soft x-ray laser intensity. At this steeper angle of incidence, most of the beam energy is absorbed in a higher density region, where the electron density gradients are too steep for optimum amplification. Also contributing to a lower laser output intensity at this angle is the shorter duration of the gain and the increased mismatch between the speed of the traveling wave of the pump, $v = c/\cos\theta$ ($v = 1.11c$ at 26°), and the amplified beam.

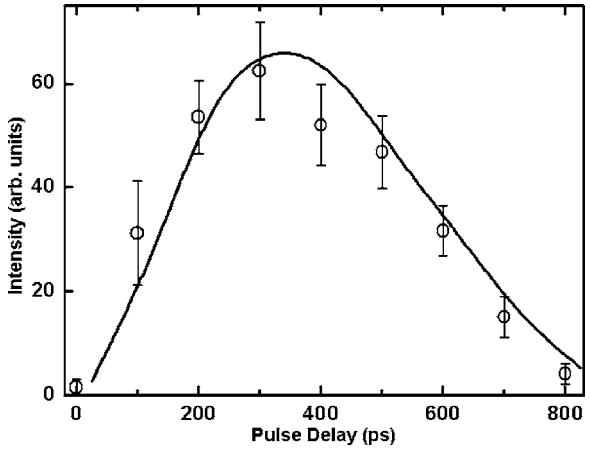

FIG. 5. Measured intensity of the 13.9 nm line of Ni-like Ag versus time delay between the 120 ps prepulse and the 8 ps grazing incidence pulse. The line is the result of a simulation conducted with the code RADEX.

Figure 5 compares the measured variation of the 13.9 nm line of Ni-like Ag line intensity as a function of delay time between the long and the short pulses with model calculations. The broad range of time delays at which strong lasing is observed (~ 100 to 600 ps) illustrates the robustness of these lasers. The Ni-like Pd laser was measured to have similar time-delay dependence. At very short delays the laser intensity decreases due to incomplete ionization by the prepulse and large refraction. The smaller volume of the gain region also plays a role. At long time delays the intensity decreases due to the lower electron densities and temperatures associated to the plasma expansion. The optimum delay was observed to decrease as a function of the ion charge Z. Figure 6 shows the variation of the intensity of the 11.9 line of Ni-like Sn as a function of delay. The optimum delay in this case, about 125 ps, is significantly shorter than the 300 ps value for Ag (Fig. 5) and the value of 700 ps previously reported for Mo [15]. This reduced optimum delay results from the fact that the high degrees of ionization necessary for lasing in higher Z ions requires hotter preplasma

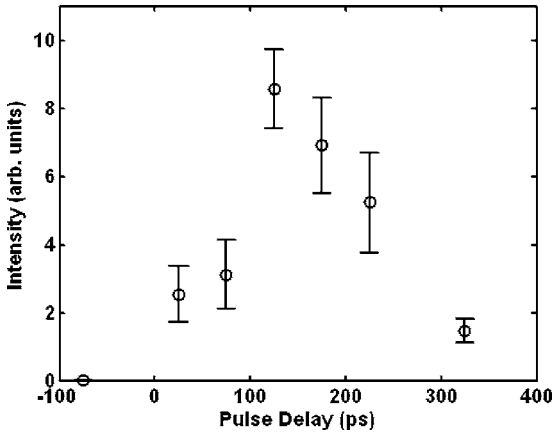

FIG. 6. Measured intensity of the 11.9 nm line of Ni-like Sn versus time delay between the 120 ps prepulse and the 8 ps grazing incidence pulse.

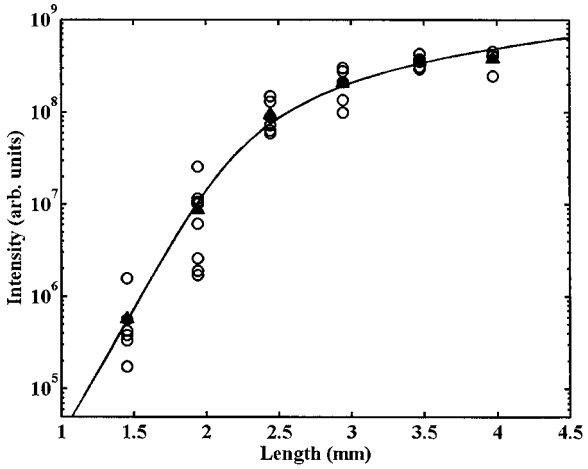

FIG. 7. Intensity versus target length for the 13.9 nm line of Ni-like Ag. The solid triangles represent the average of the points shown. A fit of the data gives a small signal gain of 67.5 cm^{-1} and a gain-length product of $gl=16.8$.

conditions, achieved only shortly after the prepulse. Therefore for lasing in higher Z ions the optimum delay that results from the tradeoff between increased Ni-like ion fraction for maximum gain coefficient and decreased electron density gradients for reduced refraction loss occurs at shorter delays.

Gain measurements were conducted for an incidence angle of 20° by monitoring the variation of the laser line intensity as a function of target length. The results for Ag are shown in Fig. 7. The 13.9 nm laser intensity is observed to increase rapidly as a function of target length, until it rolls off into saturation. The solid line corresponds to a fit of the data with an analytical expression that describes the variation of the amplified spontaneous emission as a function of plasma length taking into account the effect of gain saturation [20]. The resulting small signal gain coefficient is 67.5 cm^{-1} and $gl=16.8$. Similar gain-length products were measured for Ru, Pd, and Cd. As discussed below, higher Z elements showed progressively lower amplification. The laser pulse energy was estimated from the counts on the CCD taking into account the quantum efficiency of the detector and the losses. The energy of the most intense Ag and Pd shots obtained with a 4 mm target are estimated to exceed 0.6 μJ. Assuming the laser pulse width is that predicted by model computations, ~5 ps, and an exit beam diameter corresponding to the width of the pump beam ~30 μm, this pulse energy corresponds to a laser intensity of about 1.7×10^{10} W cm^{-2}, that exceeds the computed saturation intensity of $5-7\times10^{9}$ W/cm^2 of these lines at the plasma conditions corresponding to 20° grazing angle pumping. Figure 8 illustrates continuous 5 Hz repetition rate operation of the Ni-like Ag laser for 250 shots. The data was obtained moving the target at a velocity of 0.2 mm/s. Lasing is observed in all shots, with an intensity variation characterized by a standard deviation of ~30% of the mean. The 13.9 nm laser average power approaches 2 μW. Increased average power should be readily achieved in all these lasers by adjusting the pump laser for operation at 10 Hz repetition rate. Measurements for Ni-like Ag at a grazing-incidence pumping angle of 23° for the optimum delay of 300 ps have yielded a further increased laser output intensity, generating pulses with an energy up to 0.85 μJ. The shortest wavelength line for which amplification to gain-saturation levels was achieved is the 11.9 nm line of Ni-like Sn. Figure 9 shows the variation of the 11.9 nm laser line intensity as a function of plasma column length. The data was obtained using a main prepulse energy of ~350 mJ and a short pulse energy of ~1 J at a grazing incidence angle of 23°, at the optimum delay of 125 ps. The fit corresponds to a gain coefficient of 50 cm^{-1}, and a gain length product of $gl=14.3$, the value for which the onset of gain saturation effects are observable. The most intense 11.9 nm laser pulses were measured to have an energy of ~230 nJ. To demonstrate lasing in Ni-like Sb and Ni-like Te we reduced the FWHM length of the short pulse line focus to 3.5 mm to increase the irradiation intensity up to 1.2×10^{14} W/cm^2. Lasing was observed for delays around 70–100 ps. The large fluctuations of the shot-to-shot variation of the laser intensity prevented a reliable measurement of the gain for these materials.

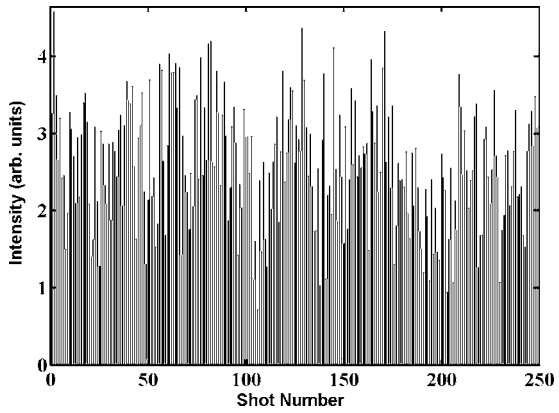

FIG. 8. Shot-to-shot variation of the intensity of the 13.9 nm Ni-like Ag laser line at 5 Hz repetition rate.

While the main focus of the work reported herein is the high repetition rate generation of gain-saturated soft x-ray laser radiation at wavelength shorter than 16.5 nm, we also

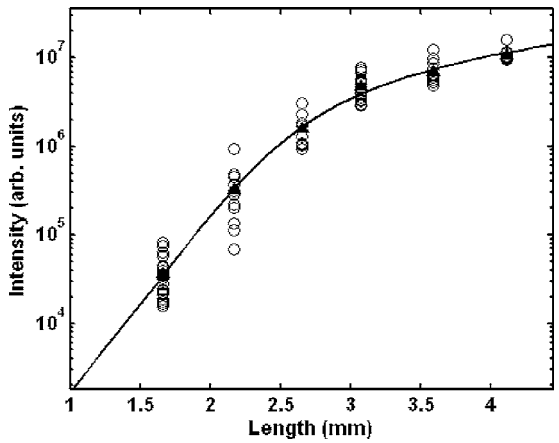

FIG. 9. Intensity as a function of target length for the 11.9 nm line of Ni-like Sn. A fit of the data gives a small signal gain of 50 cm^{-1} and a gain-length product of $gl=14.3$. The solid triangles represent the average of the points shown.

revisited the generation of 18.9 nm laser light from Ni-like Mo ions by grazing incidence pumping. An accurate measurement of the transmissivity of the thin film filters used in the experiments employing synchrotron radiation [18] showed that these filters are significantly more absorbent than what was initially estimated based on published optical constants. This suggests that the energy for the 18.9 nm wavelength Ni-like Mo laser pulses we reported in Ref. [15] for the case of grazing-incidence pumping at 14° grazing incidence is likely to be underestimated. We conducted a new Ni-like Mo laser experiment at a grazing-incidence pumping angle of 20° using 1 J of short pulse (~8 ps duration) excitation and the calibrated filters. A series of shots made using a 4 mm long Mo slab target yielded an average 18.9 nm laser pulse energy of 1 μJ, with the most intense pulses reaching 1.4 μJ. The results demonstrate the feasibility of the development of a >10 μW average power table top laser at this wavelength using 10 Hz pumping.

IV. CONCLUSIONS

In summary, soft x-ray lasers with average powers of >1 μW were demonstrated at wavelengths below 15 nm. Gain-saturated amplification at 5 Hz repetition rate was obtained in several transitions of the Ni-like isoelectronic sequence ions by efficiently heating precreated plasmas with short laser pulses of 1 J energy impinging at selected grating incidence angles. Strong amplification was obtained for wavelengths down to 11.9 nm in Ni-like Sn, transition for which a gain-length product close to saturation, $gl \sim 14$, was measured. Progressively lower gain was also obtained for wavelengths as short as 10.9 nm.

The results suggest in the near future it should be possible to operate these compact lasers for prolonged periods of time for extreme ultraviolet lithography metrology (at-wavelength interferometry of extreme ultraviolet optics and defect inspection), high resolution imaging, spectroscopy of materials, and other applications. The 2 μW laser average power level reported here at a wavelength of 13.9 nm already meets the requirements for high resolution imaging and interferometry applications which require about 1000 counts per pixel on a CCD array to produce high quality images. For the average powers reported here this amounts to exposures of a few tens of seconds [21]. Further increases in soft x-ray laser average power can be expected to result from increasing the repetition rate to 10 Hz and from additional optimization of the pump parameters.

Furthermore, based on the observation of lasing at wavelengths as short as 10.9 nm and the model simulations, we anticipate that future work should result in saturated high repetition rate table-top lasers at even shorter wavelengths.

ACKNOWLEDGMENTS

This work was supported by the NSF ERC for Extreme Ultraviolet Science and Technology under NSF Award No. EEC-0310717, with equipment developed under NSF Grant No. ECS-9977677. We also gratefully acknowledge the support of the W.M. Keck Foundation, the assistance of A. Weith with data analysis, and encouraging discussions with Jim Dunn.

[1] D. T. Attwood, *Soft X-Rays and Extreme Ultraviolet Radiation: Principles and Applications* (Cambridge University Press, Cambridge, England, 1999).
[2] G. J. Tallents, J. Phys. D **36**, 259 (2003); H. Daido, Rep. Prog. Phys. **65**, 1513 (2002).
[3] A. Paul, R. A. Bartels, R. Tobey, I. Christov, H. Kapteyn, M. Murnane, and S. Backus, Nature (London) **421**, 51 (2003).
[4] R. Smith, G. J. Tallents, J. Zhang, G. Eker, S. McCabe, G. J. Pert, and E. Wolfrum, Phys. Rev. A **59**, R47 (1999).
[5] B. R. Benware, C. D. Macchietto, C. H. Moreno, and J. J. Rocca, Phys. Rev. Lett. **81**, 5804 (1998); C. D. Macchietto, B. R. Benware, and J. J. Rocca, Opt. Lett. **24**, 1115 (1999).
[6] S. Sebban, R. Haroutunian, Ph. Balcou, G. Grillon, A. Rousse, S. Kazamias, T. Marin, J. P. Rousseau, L. Notebaert, M. Pittman, J. P. Chambaret, A. Antonetti, D. Hulin, D. Ros, A. Klisnick, A. Carillon, P. Jaegle, G. Jamelot, and J. F. Wyart, Phys. Rev. Lett. **86**, 3004 (2001); S. Sebban, T. Mocek, D. Ros, L. Upcraft, Ph. Balcou, R. Haroutunian, G. Grillon, B. Rus, A. Klisnick, A. Carillon, G. Jamelot, C. Valentin, A. Rousse, J. P. Rousseau, L. Notebaert, M. Pittman, and D. Hulin, *ibid.* **89**, 253901 (2002).
[7] D. V. Korobkin, C. H. Nam, S. Suckewer, and A. Goltsov, Phys. Rev. Lett. **77**, 5206 (1996).
[8] K. A. Janulewicz, A. Lucianetti, G. Priebe, W. Sandner, and P. V. Nickles, Phys. Rev. A **68**, 051802 (2003).
[9] P. V. Nickles, V. N. Shlyaptsev, M. Kalachinkov, M. Schnurer, I. Will, and W. Sandner, Phys. Rev. Lett. **78**, 2748 (1997).
[10] J. Dunn, Y. Li, A. L. Osterheld, J. Nilsen, J. R. Hunter, and V. N. Shlyaptsev, Phys. Rev. Lett. **84**, 4834 (2000).
[11] R. Tommasini, J. Nilsen, and E. E. Fill, Proc. SPIE **4505**, 85 (2001).
[12] T. Ozaki, R. A. Ganeev, A. Ishizawa, T. Kanai, and H. Kuroda, Phys. Rev. Lett. **89**, 253902 (2002); R. Li and Z. Z. Xu, J. Phys. IV **11**(PR2), 27 (2001).
[13] V. N. Shlyaptsev, J. Dunn, S. Moon, R. Smith, R. Keenan, J. Nilsen, K. B. Fournier, J. Kuba, A. L. Osterheld, J. J. Rocca, B. Luther, Y. Wang, and M. Marconi, Proc. SPIE **5197**, 221 (2003).
[14] R. Keenan, J. Dunn, P. K. Patel, D. F. Price, R. F. Smith, and V. N. Shlyaptsev, Phys. Rev. Lett. **94**, 103901 (2005); R. Keenan, J. Dunn, V. N. Shlyaptsev, R. Smith, P. K. Patel, and D. F. Price, Proc. SPIE **5197**, 213 (2003).
[15] B. M. Luther, Y. Wang, M. A. Larotonda, D. Alessi, M. Berrill, M. C. Marconi, V. N. Shlyaptsev, and J. J. Rocca, Opt. Lett. **30**, 165 (2005).
[16] D. Alessi, B. M. Luther, Y. Wang, M. A. Larotonda, M. Berrill, and J. J. Rocca, Opt. Express **13**, 2093 (2005).
[17] R. London. Phys. Fluids **31**, 184 (1988).
[18] Advanced Light Source, Lawrence Berkeley National Laboratory, courtesy Eric Gullikson.

[19] V. N. Shlyaptsev, A. V. Gerusov, A. V. Vinogradov, J. J. Rocca, O. D. Cortazar, F. Tomasel, and B. Szapiro, in *Ultrashort Wavelength Lasers II*, edited by S. Suckewer, SPIE Proc. Vol. 2012, pp. 99–110 (1993).

[20] G. J. Tallents, Y. Abou-Ali, M. Edwards, R. E. King, G. J. Pert, S. J. Pestehe, F. Strati, R. Keenan, C. L. S. Lewis, S. Topping, O. Guilbaud, A. Klisnick, D. Ros, R. Clarke, D. Neely, and M. Notley, in X-Ray Lasers 2002, 8th Int. Conf. on X-Ray Lasers, AIP Conf. Proc. **641**, 291 (2002).

[21] G. Vaschenko, F. Brizuela, C. Brewer, M. Grisham, H. Mancini, C. S. Menoni, M. C. Marconi, J. J. Rocca, W. Chao, J. A. Liddle, E. H. Anderson, D. T. Attwood, A. V. Vinogradov, I. A. Artioukov, Y. P. Pershyn, and V. V. Kondratenko, Opt. Lett. **30**, 2095 (2005).